Title: **Antenna-coupled spintronic terahertz emitters driven by a 1550 nm femtosecond laser oscillator**

Author(s): Nandi, U., Abdelaziz, M. S., Jaiswal, S., Jakob, G., Gueckstock, O., Rouzegar, S. M., … Preu, S.

Applied Physics Letters

Antenna-coupled spintronic terahertz emitters driven by a 1550 nm femtosecond laser oscillator

Cite as: Appl. Phys. Lett. **115**, 022405 (2019); https://doi.org/10.1063/1.5089421
Submitted: 18 January 2019 . Accepted: 15 June 2019 . Published Online: 09 July 2019

U. Nandi, M. S. Abdelaziz, S. Jaiswal, G. Jakob, O. Gueckstock, S. M. Rouzegar, T. S. Seifert, M. Kläui, T. Kampfrath, and S. Preu

Applied Physics Letters ARTICLE scitation.org/journal/apl

Antenna-coupled spintronic terahertz emitters driven by a 1550 nm femtosecond laser oscillator

Cite as: Appl. Phys. Lett. **115**, 022405 (2019); doi: 10.1063/1.5089421
Submitted: 18 January 2019 · Accepted: 15 June 2019 ·
Published Online: 9 July 2019

View Online Export Citation CrossMark

U. Nandi,[1,a)] M. S. Abdelaziz,[1] S. Jaiswal,[2] G. Jakob,[2] O. Gueckstock,[3,4] S. M. Rouzegar,[3,4] T. S. Seifert,[3,4] M. Kläui,[2] T. Kampfrath,[3,4] and S. Preu[1,b)]

AFFILIATIONS

[1]Department of Electrical Engineering and Information Technology, TU Darmstadt, 64283 Darmstadt, Germany
[2]Institute of Physics, Johannes Gutenberg University Mainz, 55099 Mainz, Germany
[3]Department of Physical Chemistry, Fritz Haber Institute of the Max Planck Society, 14195 Berlin, Germany
[4]Department of Physics, Freie Universität Berlin, 14195 Berlin, Germany

[a)]Electronic mail: nandi@imp.tu-darmstadt.de
[b)]Electronic mail: preu@imp.tu-darmstadt.de

ABSTRACT

We demonstrate antenna-coupled spintronic terahertz (THz) emitters excited by 1550 nm, 90 fs laser pulses. Antennas are employed to optimize THz outcoupling and frequency coverage of ferromagnetic/nonmagnetic metallic spintronic structures. We directly compare the antenna-coupled devices to those without antennas. Using a 200 μm H-dipole antenna and an ErAs:InGaAs photoconductive receiver, we obtain a 2.42-fold larger THz peak-peak signal, a bandwidth of 4.5 THz, and an increase in the peak dynamic range (DNR) from 53 dB to 65 dB. A 25 μm slotline antenna offered 5 dB larger peak DNR and a bandwidth of 5 THz. For all measurements, we use a comparatively low laser power of 45 mW from a commercial fiber-coupled system that is frequently employed in table-top THz time-domain systems.

Classic electronic applications make use of the charge of the electron, as manifested by a large range of circuit elements and devices that dominate today's circuitry. Spintronic devices, on the other hand, take additional advantage of the spin of the electron.[1] Recently, the speed of elementary spintronic operations such as the generation of spin currents and their conversion into charge currents[2,3] has been pushed into the terahertz (THz) frequency range.[4–9]

A promising application emerging from these efforts are spintronic THz emitters (STEs) consisting of a stack of ferromagnetic (FM) and nonferromagnetic (NM) metal thin films[4,5] [see Fig. 1(a)]. Upon excitation with a femtosecond laser pulse, spin angular momentum is transferred from the FM into the NM layer.[10] In the latter, the out-of-plane-directed spin current of density j_s is converted into an in-plane charge current with density j_c by means of the inverse spin Hall effect[2,3] (ISHE). The ultrafast charge flow, in turn, acts as a source of broadband electromagnetic radiation with frequencies extending into the THz range.

STEs have promising properties such as larger bandwidth and conversion efficiency than optical-rectification crystals such as ZnTe and GaP,[5] output scalability while maintaining low fabrication costs,[9] insensitivity to the pump wavelength,[11,12] and flexible substrates.[6] Therefore, such devices are excellent candidates for applications in THz time-domain spectroscopy systems.[13]

To further improve STE performance, one needs to increase (i) the local amplitude of the charge-current density j_c and (ii) the far-field coupling of the emitting structure. Regarding (i), the THz signal amplitude for a given incident pump power P_{pump} was optimized by decreasing the total metal-film thickness[5] (for increased deposited energy density), by varying the FM material[5,6,14] (to maximize the spin current) and the material and location of the NM layers[5,6,15,16] (to maximize spin-to-charge conversion), and by using photonic structures[12,17] (for enhanced optical absorption). Concerning (ii), antennas are frequently used to improve the radiation efficiency and to maximize the power emitted by a source current j_c. While such antennas are routinely used in state-of-the-art semiconductor-based photoconductive THz emitters and receivers,[18–21] they have not yet been employed for metallic emitters such as STEs.

In this paper, we demonstrate antenna-coupled STEs excited with 1550 nm, 90 fs, 100 MHz laser pulses at fairly low average power levels of 45 mW that are available from commercial table-top fiber-coupled laser systems. The performance of various antenna types is compared to plain STEs in terms of their emission and pump-power saturation characteristics.

We start with a brief theoretical consideration of antenna-based THz sources. The in-plane current distribution j_c [Fig. 1(b)] of the

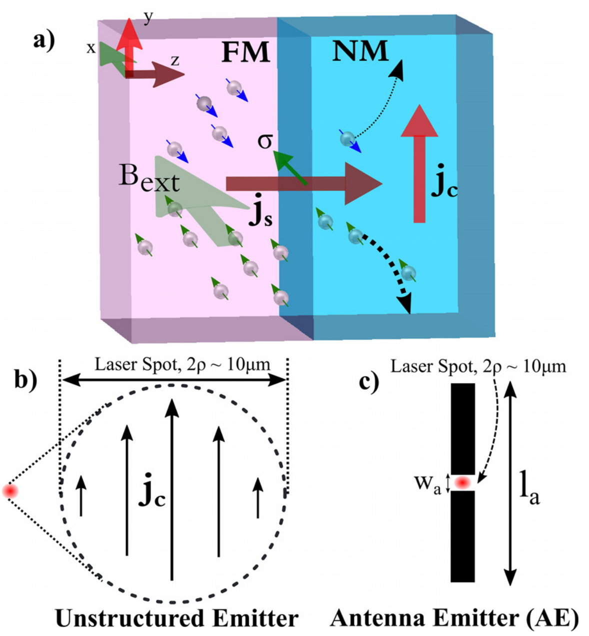

FIG. 1. Schematic of THz emission from photoexcited FM—NM bilayers, plain and microstructured. (a) A femtosecond laser pulse triggers ultrafast spin transport from the FM into the NM layer where the spin current j_s flowing along the z axis is converted into a charge current j_c along the y direction, acting as a source of THz radiation. The direction of the in-plane magnetization of the FM layer is set along the x axis by an external magnetic field B_{ext}. (b) Current distribution in an unstructured (plain) bilayer and (c) the STE bilayer embedded in the gap of an antenna. Note that THz current generation by the ISHE is independent of emitter type and antenna choice.

emitter can be considered as an electric dipole whose moment has magnitude $\mu \sim \bar{j}_c d\rho^2/\omega$. Here, $\bar{j}_c$, ρ, and d are the spatial average, the radius, and the thickness of the current distribution j_c, respectively, while $\omega/2\pi$ is the frequency of the THz wave. Note that the dipole moment μ is independent of the radius ρ because j_c is proportional to the pump intensity $j_c \sim P_{pump}/\rho^2$ in the linear fluence regime.

To determine the emitted THz power for a given P_{pump} and, thus, μ, we first consider the case of a pump spot much larger than the emitted wavelength $\lambda_{THz} = 2\pi c_0/\omega$, that is, $\rho \gg \lambda_{THz} \sim 100\,\mu$m, where c_0 denotes the vacuum speed of light. The resulting THz beam is highly collimated and, thus, directed. It carries a power of $P \sim Z_0 \bar{j}_c^2 d^2 \rho^2 \propto Z_0 \mu^2 \omega^2/\rho^2$, where $Z_0 = 377\ \Omega$ is the free-space impedance.[15] While this result suggests us to make ρ as small as possible, it neglects two effects: first, the pump intensity has to remain below the damage threshold of the STE. Second, for a spot radius much smaller than the THz wavelength, the spatial frequency spectrum of the planar j_c distribution is dominated by evanescent components that do not carry electromagnetic energy to the far-field.[15] More precisely, for $\rho \ll \lambda_{THz}$, which is often used in the case of laser oscillators,[5] the current distribution j_c should be considered as an electric point dipole with moment μ [see Fig. 1(b)]. It emits a power of $P \propto Z_0 \mu^2 \omega^4$, which is now independent of the pump-spot radius ρ.

To mitigate this poor scaling behavior, we place the current distribution j_c, so far located in an in-plane homogeneous environment [see Fig. 1(b)], in the center of an antenna structure (AE) with gap size w_a [see Fig. 1(c)]. The current density j_c feeds the antenna arms of length l_a and, thus, effectively increases the current-carrying surface by a factor of $\sim l_a/\rho$. As a consequence, the wide spatial frequency spectrum of j_c is transformed into a narrower and more radiative one. The price to pay is losses related to feeding of the antenna.[22]

In the case of an electrically short antenna ($l_a \ll \lambda$), the antenna is expected to increase the THz power emitted by a subwavelength current distribution as compared to the unstructured emitter by a factor of

$$\frac{P_{AE}}{P_{plain}} \sim \frac{l_a^2}{w_a^2}. \tag{1}$$

A more accurate consideration, taking the radiation resistance of the antenna into account, is detailed in the supplementary material. The enhancement factor due to an arbitrary antenna becomes

$$\frac{P_{AE}}{P_{plain}} = \frac{\eta_{prop}\eta_{circ}R_a}{789\Omega \cdot n_{eff}} \cdot \left(1 + \frac{\omega^2}{\omega_\rho^2}\right) \cdot \left(\frac{2\pi c_0}{\omega w_a}\right)^2. \tag{2}$$

Here, n_{eff} is the effective refractive index of the substrate and

$$\eta_{circ}(\omega) = \frac{R_s^2}{(R_s + R_a)^2 + X_a^2}, \tag{3}$$

where R_s is the resistance of the spintronic layer (about 100–130 Ω for the antenna-coupled devices studied in this work), R_a is the real (radiating) part of the antenna impedance, and X_a is its imaginary (near-field-related) part. The second factor in Eq. (2) is only relevant for large illumination areas. As the characteristic frequency $\omega_\rho = \sqrt{6}c/(n_{eff}\rho) \gg \omega$ for the cases discussed in this paper, this term can be omitted. The term $\eta_{prop}(\omega)$ accounts for the frequency-dependent propagation of the THz signal from the source to the receiver, as well as for antenna-coupling effects.

To implement antenna-enhanced THz emission from STEs, we use samples as schematically shown in Fig. 2(a). The fabricated STE consists of a trilayer metallic structure Pt(2 nm)|$Co_{40}Fe_{40}B_{20}$(1.8 nm)|W(2 nm) where the FM layer ($Co_{40}Fe_{40}B_{20}$) is sandwiched between two NM layers (Pt and W) with opposite spin Hall angles ($\gamma > 0$ and $\gamma' < 0$). Consequently, the charge currents in the two NM layers add up constructively, thereby increasing the THz field amplitude by 40% compared to a $Co_{40}Fe_{40}B_{20}$|Pt bilayer.[5] The metal composition and the thickness of the individual metal layers were optimized to obtain maximum THz emission.[5] The metal stack is deposited on a Si(280 μm)|SiO_x(0.3 μm) wafer with highly resistive Si (resistivity of ∼10 kΩ cm). The SiO_x was incorporated to enable DC biasing of the spintronic layers without any leakage current from the Si. Its effect on THz emission will be discussed in a separate publication.

Two antenna types [Fig. 2(b)], a slotline (spacing of 25 μm) and an H-dipole (a length of $l_a = 200\,\mu$m and a gap size of $w_a = 10\,\mu$m), consisting of Ti(20 nm)|Au(150 nm), were deposited on the spintronic stack and structured using ultraviolet photolithography, evaporation, and lift-off techniques. The parallel metallic lines feature a width of 10 μm in both cases. Subsequently, the spintronic trilayer stack was removed by argon-plasma sputter etching, except for the illuminated area of the antenna gap and a small width around the antenna arms [see Fig. 2(b)]. To increase the coupling of pump light into the

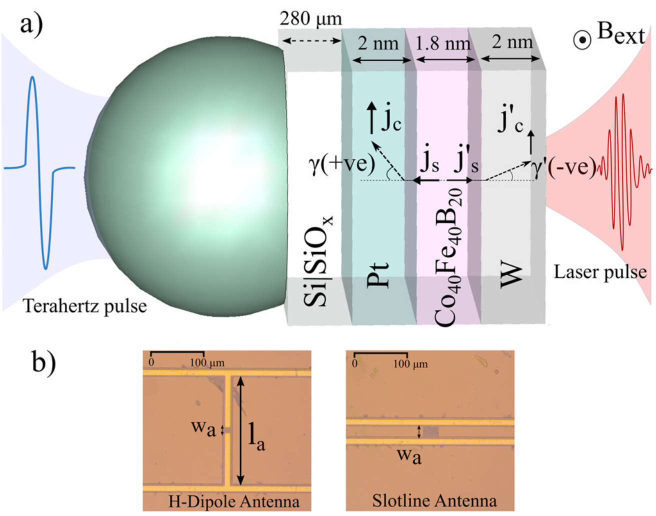

FIG. 2. (a) Schematic of the spintronic THz emitter (STE) consisting of a Pt(2 nm)|$Co_{40}Fe_{40}B_{20}$(1.8 nm)|W(2 nm) trilayer on a Si(280 μm)|SiOx(0.3 μm) substrate. The incident femtosecond laser pulse triggers spin currents j_s and j_s' into the Pt and W layers in which they are converted into charge currents j_c and j_c'. The THz wave emitted by j_c and j_c' is collected and collimated by a hyperhemispherical silicon lens. Optionally, a THz antenna structure is deposited on top of the spintronic trilayer. (b) Micrographs of two fabricated antenna-coupled devices as seen from the right-hand side in panel (a): an STE coupled to an H-dipole ($l_a = 200\,\mu$m and gap size of $w_a = 10\,\mu$m) (left) and a slotline (right) antenna ($w_a = 25\,\mu$m). The antennas consist of gold (yellow) with the spintronic stack in its center (grayish brown).

spintronic trilayer, an antireflection coating layer of SiN was deposited over the entire antenna structure (excluding the contact pads not shown in the figure), resulting in an absorption of about 80% ± 10% of the incident 1550 nm laser power in the metal layers.[12] Finally, the emitters were mounted on a hyperhemispheric Si lens (radius of 5 mm with a hyperhemispheric offset of 1.38 mm including the substrate) for improved outcoupling of the THz radiation through the Si-air interface [Fig. 2(a)].

Our measurement system is a THz time-domain spectroscopy setup using a pulsed laser (modified Menlo C-fiber, a center wavelength of 1560 nm, a pulse duration of 90 fs, and a repetition rate of 100 MHz) as detailed in Ref. 20. An ErAs:InGaAs photoconductor with an H-dipole antenna (a width of 25 μm and a gap of 5 μm) was used as the receiver, similar to that in Ref. 20. The entire system was operated with fiber-coupled laser pulses at an average power of 45 mW for the STE and 16 mW for the ErAs:InGaAs receiver. The optical power is limited by excessive nonlinear fiber dispersion that appears at higher power levels. To determine the damage threshold of the STEs, we further used a free-space port with up to 350 mW laser power. The external magnetic field B_{ext} [Fig. 2(a)] was applied by two permanent magnets with a distance of approximately 5 cm symmetrically around the sample. It was chosen to be strong enough to saturate the magnetization, as confirmed by using four different sets of magnets with varying field strengths.

We first determined the optimum working point of the devices in terms of pump power. For this purpose, we measured the emitted THz field strength as a function of P_{pump} using H-dipole antennas with a gap of 10 μm and a length of 50 μm. A tightly focused laser spot with an estimated laser spot size of $2\rho \approx 10 \pm 4\,\mu$m was used for the free-space port. By increasing the laser power, the THz amplitude initially increased monotonically and eventually saturated at about 100 mW (Fig. 3). Upon further increase in the laser power, an irreversible drop of the THz amplitude was observed (Fig. 3). Microscopy inspection revealed a slight change in color (although the metal film was still intact), indicating damage to the structure. This effect may result from thermally driven diffusion of atoms between the metallic layers. We note that the SiO_x layer currently impedes heat transfer to the thermally well conducting Si substrate, which can be mitigated by omitting this layer or just reducing its thickness. We emphasize, however, that for the laser power of 45 mW available from the fiber-coupled port, we did not observe noticeable saturation of the THz field strength. We conclude that our current devices are well compatible with state-of-the-art table-top fiber-coupled laser systems.

Having determined the optimum working point of our STEs, we now turn to the major goal of this study and compare the output power of antenna-coupled devices to that of excitation of a plain spintronic trilayer. Figure 4 shows the central result of this work: the THz signals as obtained from an unstructured STE and two antenna-coupled devices under otherwise identical experimental conditions using the fiber-coupled laser signals. The time-domain signals are displayed in Fig. 4(a). While the peak-to-peak signal from the plain STE is 65 mV, significantly enhanced peak-to-peak signals are observed for the antenna-coupled devices, with a maximum of 157 mV using the H-dipole antenna with $l_a = 200\,\mu$m and $w_a = 10\,\mu$m. Therefore, this antenna enhances the emitted THz power by a factor of $2.42^2 \approx 5.86$ as compared to the unstructured emitter.

The spectral characteristics of the emitters can be studied following a Fourier transformation of the time-domain signals. Figures 4(b) and 4(c) show the power spectra of the plain emitter (P_{plain}) compared to those of the antenna-coupled devices (P_{AE}): the 200 μm H-dipole and the 25 μm slotline, respectively. The plain emitter shows a dynamic range (DNR) of 53 dB with a 4.5 THz bandwidth. The 200 μm H-dipole achieves a maximum DNR of 65 dB which is 12 dB greater than the DNR of the unstructured emitter with the same bandwidth of about 4.5 THz [Fig. 4(b)]. To achieve a similar DNR with the unstructured emitter, an about 4 times higher laser power would be

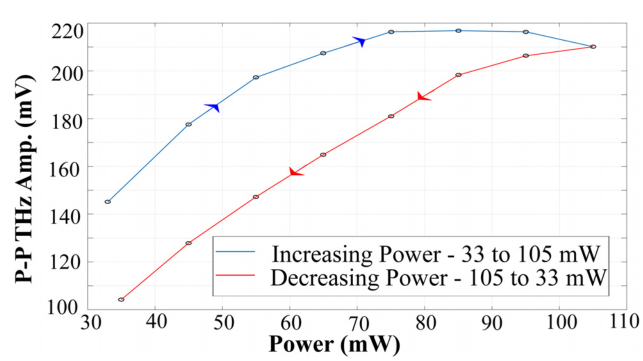

FIG. 3. Emitted THz signal (peak-to-peak) vs incident laser power. The measurement was for an H-dipole antenna with a gap of 10 μm and a length of 50 μm. The laser power was increased gradually (blue curve) and, after having reached its maximum, decreased again (red curve).

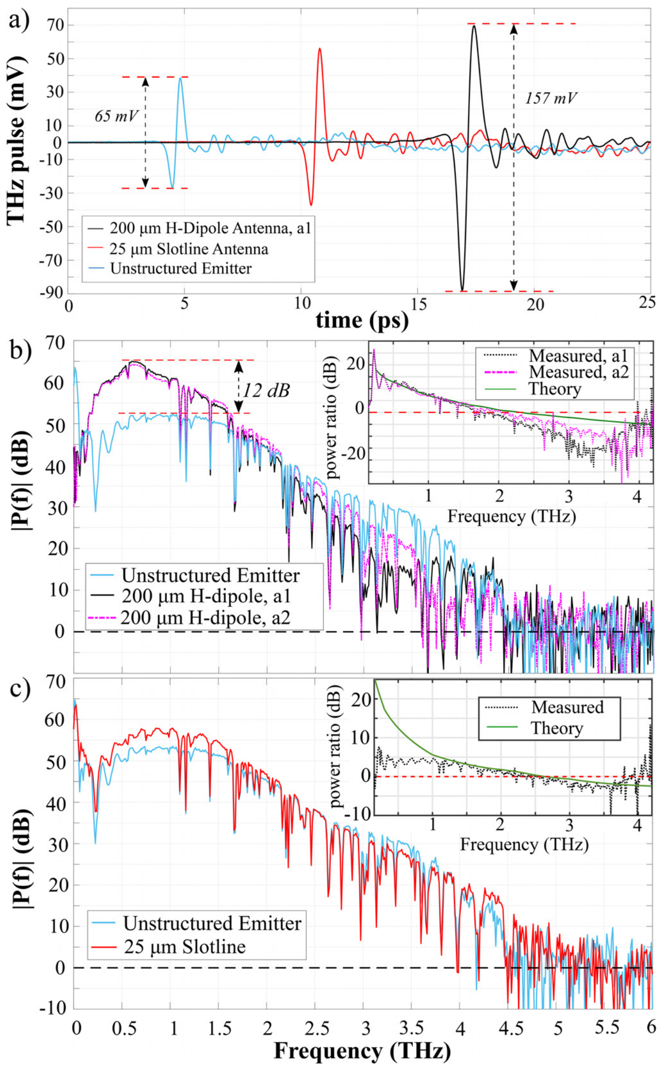

FIG. 4. Performance of antenna-coupled STEs. (a) Time domain signals as obtained from a plain STE and the devices coupled to a 25 μm slotline and a 200 μm-wide H-dipole antenna. Waveforms are offset horizontally for clarity. (b) Power spectrum of the 200 μm H-dipole-antenna-based STE (P_{AE}) vs the plain STE (P_{plain}). Two different alignments have been used: a1 is optimized for low frequencies [also shown in panel (a)], a2 for frequencies above 2 THz. Dips in the spectra predominantly arise from absorption by water vapor. The inset shows the ratio P_{AE}/P_{plain} as obtained from the experiment and from our modeling based on Eq. (2). (c) As panel (b), but for the 25 μm slotline antenna.

required, i.e., about 180 mW, which is hardly achievable within fibers while preserving a pulse duration of 90 fs.

The differences in the spectral characteristics of the H-dipole as compared to the unstructured emitter can be rationalized based on the frequency-dependent radiation impedance $Z_a = R_a + iX_a$ of the antenna. The spectral sensitivity of our measurement system, defined through the laser pulse duration and the ErAs:InGaAs receiver response, is the highest at frequencies below 1 THz. Owing to the much higher R_a of the H-dipole antenna at frequencies below 1 THz as compared to the unstructured emitter, these frequency components are enhanced by the antenna-coupled emitter, leading to an increase in the dynamic range of 12 dB and the peak-to-peak THz pulse amplitude in the time domain by a factor of 2.42 [Fig. 4(a)].

For the slotline, on the other hand, the current generated in the gap first flows vertically to the metal lines, emitting THz radiation the same way as the unstructured device. Currents flowing within the metal lines emit very little radiation in the direction of the receiver at low THz frequencies at which the distance between the metal lines is a fraction of the wavelength. In addition, the fields generated by the current flowing within the two metal lines cancel in the far field along the receiver direction. Therefore, there is comparatively little difference in the emitted spectrum of the slotline and the unstructured device. The slightly larger peak DNR of about 5 dB and an extended bandwidth of 5 THz [Fig. 4(c)] is due to some contribution of radiation from the metal lines, particularly at higher THz frequencies where they become radiative.

To compare the measured spectra to theory [Eq. (2)], the insets of Figs. 4(b) and 4(c) display the ratio P_{AE}/P_{plain} vs frequency, that is, the power spectrum of the antenna-coupled STEs normalized by that of the plain STE. The theoretical results based on Eq. (2) and simulated radiation impedances of the antennas using CST microwave studio are shown as well. The model also accounts for the far-field radiation patterns of the various emitter structures. For the H-dipole [Fig. 4(b) inset], we find excellent agreement between experiment and theory, both in terms of frequency dependence and absolute values, even though the propagation from the source to the receiver was not simulated. Nonideal THz propagation and coupling to the receiver antenna (e.g., due to different alignments) noticeably change the spectrum, as is shown for an alignment emphasizing low [(a1) in the inset of Fig. 4(b)] and high frequency components [(a2)]. The spectral differences of the two alignments are larger than the deviation to the theoretical model. For the slotline antenna [inset of Fig. 4(c)], the simulation does not as well reproduce the propagation of frequency components below 1 THz. Therefore, the performance below 1 THz is currently not understood. However, above 1 THz, the theoretical model again excellently agrees with the experimental findings.

In conclusion, we demonstrated and characterized lumped-element, antenna-coupled STEs under pulsed operation with an ErAs:InGaAs photoconductor as the receiver. The inexpensive, compact, and portable antenna-coupled devices are well suited for THz generation with commercial fiber laser systems at 1550 nm. We have shown that a laser power as low as 45 mW is sufficient to operate the devices with high DNR of up to 65 dB. All antennas led to a significant increase in the THz output as compared to plain, unstructured emitters. A maximum amplitude increase in 2.42 of the peak-to-peak THz time-domain signal was obtained using the 200 μm H-dipole antenna, corresponding to an increase in the DNR by 12 dB. Our results indicate that antenna coupling of STEs is a promising route for further enhancement of the output amplitude and tailoring of the bandwidth of this class of THz emitters for both free-space and on-chip THz applications.

See the supplementary material for the derivation of the ratio of power emitted by antenna emitters and the unstructured emitter.

This research was funded by the Deutsche Forschungsgemeinschaft (DFG, German Research Foundation) through Project Nos. 290319996/TRR173, 318612841, and 278381540/

PR1413/3-1 (REPHCON) and project B02 of the SFB/TRR227 Ultrafast Spin Dynamics. We further acknowledge CST for the EM Simulation solver.

REFERENCES

[1]J. Sinova, S. O. Valenzuela, J. Wunderlich, C. H. Back, and T. Jungwirth, "Spin Hall effects," Rev. Mod. Phys. **87**(4), 1213 (2015).
[2]E. Saitoh, M. Ueda, H. Miyajima, and G. Tatara, "Conversion of spin current into charge current at room temperature: Inverse spin-Hall effect," Appl. Phys. Lett. **88**(18), 182509 (2006).
[3]S. O. Valenzuela and M. Tinkham, "Direct electronic measurement of the spin Hall effect," Nature **442**(7099), 176 (2006).
[4]T. Kampfrath, M. Battiato, P. Maldonado, G. Eilers, J. Nötzold, S. Mährlein, V. Zbarsky, F. Freimuth, Y. Mokrousov, S. Blügel *et al.*, "Terahertz spin current pulses controlled by magnetic heterostructures," Nat. Nanotechnol. **8**(4), 256 (2013).
[5]T. Seifert, S. Jaiswal, U. Martens, J. Hannegan, L. Braun, P. Maldonado, F. Freimuth, A. Kronenberg, J. Henrizi, I. Radu *et al.*, "Efficient metallic spintronic emitters of ultrabroadband terahertz radiation," Nat. Photonics **10**(7), 483–488 (2016).
[6]D. Yang, M. Elyasi, X. Qui, M. Chen, Y. Liu, L. Ke, and H. Yang, "Powerful and tunable THz emitters based on the Fe/Pt magnetic heterostructure," Adv. Opt. Mater. **4**(12), 1944 (2016).
[7]G. Torosyan, S. Keller, L. Scheuer, R. Beigang, and E. Th. Papaioannou, "Optimized spintronic terahertz emitters based on epitaxial grown Fe/Pt layer structures," Sci. Rep. **8**(1), 1311 (2018).
[8]T. J. Huisman, R. V. Mikhaylovskiy, J. D. Costa, F. Freimuth, E. Paz, J. Ventura, P. P. Freitas, S. Blügel, Y. Mokrousov, T. Rasing *et al.*, "Femtosecond control of electric currents in metallic ferromagnetic heterostructures," Nat. Nanotechnol. **11**(5), 455 (2016).
[9]T. Seifert, S. Jaiswal, M. Sajadi, G. Jakob, S. Winnerl, M. Wolf, M. Kläui, and T. Kampfrath, "Ultrabroadband single-cycle terahertz pulses with peak fields of 300 kV cm^{-1} from a metallic spintronic emitter," Appl. Phys. Lett. **110**(25), 252402 (2017).
[10]M. Battiato, K. Carva, and P. M. Oppeneer, "Superdiffusive spin transport as a mechanism of ultrafast demagnetization," Phys. Rev. Lett. **105**(2), 027203 (2010).
[11]E. T. Papaioannou, G. Torosyan, S. Keller, L. Scheuer, M. Battiato, V. K. Magusara, J. L'huillier, M. Tani, and R. Beigang, "Efficient terahertz generation using Fe/Pt spintronic emitters pumped at different wavelengths," IEEE Trans. Magn. **54**, 1–5 (2018).
[12]R. I. Herapath, S. M. Hornett, T. S. Seifert, G. Jakob, M. Kläui, J. Bertolotti, T. Kampfrath, and E. Hendry, "Impact of pump wavelength on terahertz emission of a cavity-enhanced spintronic trilayer," Appl. Phys. Lett. **114**(4), 041107 (2019).
[13]R. L. Milot, M. T. Klug, C. L. Davies, Z. Wang, H. Kraus, H. J. Snaith, M. B. Johnston, and L. M. Herz, "The effects of doping density and temperature on the optoelectronic properties of formamidinium tin triiodide thin films," Adv. Mater. **30**(44), 1804506 (2018).
[14]T. Seifert, U. Martens, S. Günther, M. H. Aguirre, P. A. Algarabel, A. Anadón, H. S. Körner, J. Walowski, C. Back, M. R. Ibarra *et al.*, "Terahertz spin currents and inverse spin Hall effect in thin-film heterostructures containing complex magnetic compounds," SPIN **7**(03), 1740010 (2017).
[15]T. Seifert, N. M. Tran, O. Gueckstock, S. M. Rouzegar, L. Nadvornik, S. Jaiswal, G. Jakob, V. V. Temnov, M. Münzenberg, M. Wolf *et al.*, "Terahertz spectroscopy for all-optical spintronic characterization of the spin-Hall-effect metals Pt, W and $Cu_{80}Ir_{20}$," J. Phys. D **51**(36), 364003 (2018).
[16]Y. Sasaki, K. Z. Suzuk, and S. Mizukami, "Annealing effect on laser pulse-induced THz wave emission in Ta/CoFeB/MgO films," Appl. Phys. Lett. **111**(10), 102401 (2017).
[17]Z. Feng, R. Yu, Y. Zhou, H. Lu, W. Tan, H. Deng, Q. Lui, Z. Zhai, L. Zhu, J. Cai *et al.*, "Highly efficient spintronic terahertz emitter enabled by metal-dielectric photonic crystal," Adv. Opt. Mater. **6**, 1800965 (2018).
[18]S. Preu, "A unified derivation of the terahertz spectra generated by photoconductors and diodes," J. Infrared, Millimeter, Terahertz Waves **35**(12), 998–1010 (2014).
[19]R. B. Kohlhaas, R. J. B. Dietz, S. Breuer, S. Nellen, L. Liebermeister, M. Schell, and B. Globisch, "Improving the dynamic range of InGaAs-based THz detectors by localized beryllium doping: Up to 70 dB at 3 THz," Opt. Lett. **43**(21), 5423–5454 (2018).
[20]U. Nandi, J. C. Norman, A. C. Gossard, H. Lu, and S. Preu, "1550-nm driven ErAs: In (Al) GaAs photoconductor-based terahertz time domain system with 6.5 THz bandwidth," J. Infrared, Millimeter, Terahertz Waves **39**(4), 340–348 (2018).
[21]N. T. Yardimci, S. H. Yang, C. W. Berry, and M. Jarrahi, "High-power terahertz generation using large-area plasmonic photoconductive emitters," IEEE Trans. Terahertz Sci. Technol. **5**(2), 223–229 (2015).
[22]S. Preu, G. H. Döhler, S. Malzer, L. J. Wang, and A. C. Gossard, "Tunable, continuous-wave terahertz photomixer sources and applications," J. Appl. Phys. **109**(6), 061301 (2011).